The Impact of Flexural/Torsional Coupling on the Stability of Symmetrical Laminated Plates

Hafid Mataich* and Bouchta El Amrani

Laboratory of Mathematics, Modeling and Applied Physics, High Normal School, Sidi Mohamed Ben Abbellah University, 30040 Fez, Morocco
E-mail: hafid.mataich@usmba.ac.ma; bouchta.elamrani@usmba.ac.ma
**Corresponding Author*

Received 23 March 2023; Accepted 04 December 2023;
Publication 29 December 2023

Abstract

In this study, we will evaluate the effect of bending/torsion coupling on the buckling instability and free vibration behavior of symmetrical laminated plates. We will load these plates in-plane with bi-axial or uni-axial, uniform or non-uniform mechanical loads. To quantify this behavior, we'll compare the results obtained with those of specially orthotropic symmetrical plates (where bending/torsion coupling is absent). A parametric study will be carried out by varying the plate's aspect ratio, anisotropy ratio and/or lamination angle. The aim of these studies is to construct a planar loading margin for the plate while remaining elastically stable, and to determine a physically admissible limit where we can approximate the behavior of symmetrical laminates to that of specially orthotropic plates (easy to study). We will base ourselves on a Rayleigh-Ritz energy formulation of the problem because of the difficulty of finding closed-form solutions. Following validation of this formulation,

European Journal of Computational Mechanics, Vol. 32_5, 441–466.
doi: 10.13052/ejcm2642-2085.3251

a numerical survey of the results will be carried out to quantify the effect of bending/torsion coupling on the instability of this type of plate. Various conditions on the plate boundaries will be used.

Keywords: Static instability, buckling, coupling, natural frequency, critical load, Rayleigh, Ritz method.

1 Introduction

Rectangular laminated plates made of composite materials are combined structures of a first material (matrix) reinforced by another material with powerful properties (fibers). These plates are the most widespread and practical elements for the construction of structures in aeronautics as well as in a vast industrial field [1, 2], so the study of their static stability and free dynamic behavior is of crucial interest. Indeed, when a plate is statically loaded in its plane, there comes a time when transverse displacement is no longer a linear function of the applied excitations. Perhaps these displacements even become very dangerous under infinitesimally small external disturbances. So it's impossible for the engineer not to know the conditions under which a critical load that triggers the elastic instability of a plate is reached. In the open literature, many researchers have focused on the study of plate elastic instability, [3–6] have studied the buckling of plates made of FGM functional gradient materials, [7–12] propose models for studying the buckling of rolled plates. Similarly, the treatment of the free vibratory behavior of the plate leads to the determination of the natural frequencies at which the plate vibrates in the resonance regime. Consequently, in the literature of works that deal with the free dynamics of plates such as [13–17] which study the instability of plates in free vibration, [18] uses a three-dimensional method for the analysis of the dynamic stability of a plate. Thermal excitation and its effect on plate stability in both buckling and free dynamics is a topic that is taking its place in the literature, with researchers [19–30] using the thermal field as an external excitation and looking for different critical values of structural stability.

In this paper, we investigate quantitatively the effect of mutual coupling between the flexural/torsional behaviors of a symmetrical laminated plate with angular folds,[1] on the buckling stability and free vibration of this type

[1]The layers are symmetrical with respect to the neutral plane of the laminate, with the orientation angle of the reinforcing fibers in the laminate strictly greater than 0° and strictly less than 90°.

of plate. In fact, the presence of the non-zero flexural/torsional coupling stiffnesses D_{16} and D_{26} is one factor, among others, influencing the operating stability of these plates. Furthermore, we know that in the elasticity of laminated plates, the flexural/torsional coupling coefficients D_{16} and D_{26} are inversely proportional to the number of layers making up the plate. To understand this effect, we compare the stability of the symmetrical, angularly-folded laminated plates studied here with that of a specially orthotropic laminate with no flexural/torsional coupling ($D_{16} = D_{26} = 0$) [31]. The impact of buckling load and natural frequency depends, as we shall see in this study, on geometry, material properties [32, 33], and the way the plate is loaded. In a parametric study, all these effects will be taken into account.

On the other hand, in a situation that verifies simply supported boundary conditions, we can explain exact analytical solutions based on Navier's sine series developments [34], which is possible if there is no flexural/torsional coupling. On the other hand, if we analyze plates with various boundary conditions (simple supports, embedded, free, ... etc.), and/or for symmetrical lamination with which we have flexural/torsional coupling, exact closed-form analytical solutions will be impossible. For these reasons, we have choices between numerical or semi-numerical solution methods such as the Rayleigh-Riz method [35–38] adopted in this article.

2 Mathematical Formulation of the Problem

2.1 Deflection Equation Taking Account of Elastic Buckling Instability

Let's consider a laminated plate with a thin rectangular shape (Kirchhoff-Love assumptions are adopted), overall thickness h, length b and width a, composed of layers N_c symmetrical layers with respect to the neutral plane, the main coordinates of the fibers (x^k, y^k, z^k) linked to the k$^{\text{ème}}$ layer are oriented at an angle θ^k to the axes of the plate reference frame $(\hat{x}, \hat{y}, \hat{z})$ referred to as the global or problem frame (see Figure 1a). The positive z-axis is oriented upwards, so that the ordinates of the k-layer are $z = z_k$ and $z = z_{k+1}$ (see Figure 1b).

The equation of motion of a thin symmetrical laminated plate (no in-plane coupling $B_{ij} = 0$) governing transverse deflection (1) is decoupled from those governing in-plane membrane displacements (readers interested in knowing where these equations come from can consult [1]). In this study, the plate buckling analysis assumes that the only applied loads are in-plane

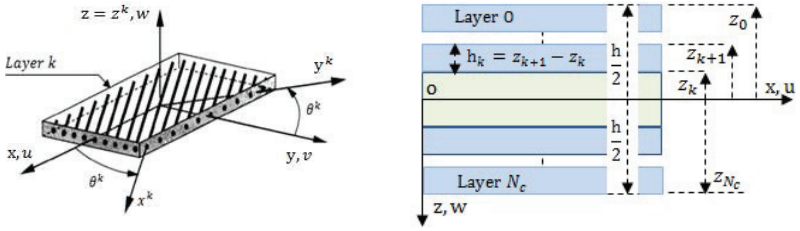

(a): Cartesian coordinates of k-layer (b): Layer ordinates and numbering

Figure 1 Diagram of a laminated plate made of the composite material studied.

forces and that all other mechanical/thermal loads are zero. Whereas, the free vibration analysis assumes that all loads are zero. The equilibrium equation governing buckling deformation w is given for a linear analysis, as

$$\begin{aligned} &D_{11}\mathrm{w}_{,xxxx} + 4D_{16}\mathrm{w}_{,xxxy} + 2(D_{12} + 2D_{66})\mathrm{w}_{,xxyy} + 4D_{26}\mathrm{w}_{,xyyy} \\ &\quad + D_{22}\mathrm{w}_{,yyyy} - \mathrm{F}_x\mathrm{w}_{,xx} - 2\mathrm{F}_{xy}\mathrm{w}_{,xy} - \mathrm{F}_y\mathrm{w}_{,yy} \\ &\quad = I_0 w_{,tt} - I_2(w_{,xx} + w_{,yy})_{,tt} \end{aligned} \tag{1}$$

With $D_{ij}, (ij = 11, 12, 22, 16, 26, 66)$ are the bending stiffness coefficients of the plate, with

$$D_{ij} = \sum_{k=1}^{N_c} \int_{z_{k-1}}^{z_k} \overline{Q}_{ij}^{(k)} z^2 dz \tag{2}$$

$\overline{Q}_{ij}^{(k)}$ are the stiffness coefficients of layer number k transformed into the global laminate reference frame $(\hat{x}, \hat{y}, \hat{z})$ their expressions are:

$$\overline{Q}_{11}^{(k)} = Q_{11}cos^4\theta^{(k)} + 2(Q_{12} + 2Q_{66})cos^2\theta^{(k)}sin^2\theta^{(k)} + Q_{22}sin^4\theta^{(k)}$$

$$\overline{Q}_{12}^{(k)} = Q_{12}cos^4\theta^{(k)} + (Q_{11} + Q_{22} - 4Q_{66})cos^2\theta^{(k)}sin^2\theta^{(k)} + Q_{12}sin^4\theta^{(k)}$$

$$\overline{Q}_{22}^{(k)} = Q_{22}cos^4\theta^{(k)} + 2(Q_{12} + 2Q_{66})cos^2\theta^{(k)}sin^2\theta^{(k)} + Q_{11}sin^4\theta^{(k)}$$

$$\begin{aligned} \overline{Q}_{16}^{(k)} &= (Q_{11} - Q_{12} - 2Q_{66})cos^3\theta^{(k)}sin\theta^{(k)} \\ &\quad + (2Q_{66}^{(k)} + Q_{12} - Q_{22})cos\theta^{(k)}sin^3\theta^{(k)} \end{aligned}$$

$$\begin{aligned} \overline{Q}_{26}^{(k)} &= (Q_{11} - Q_{12} - 2Q_{66})cos\theta^{(k)}sin^3\theta^{(k)} \\ &\quad + (2Q_{66} + Q_{12} - Q_{22})cos^3\theta^{(k)}sin\theta^{(k)} \end{aligned}$$

$$\overline{Q}_{66}^{(k)} = (Q_{11} + Q_{22} - 2Q_{12} - 2Q_{66})cos^2\theta^{(k)}sin^2\theta^{(k)} + Q_{66}(cos^4\theta^{(k)} + sin^4\theta^{(k)}) \quad (3)$$

Q_{ij} are the stiffness coefficients of the material in the (x^k, y^k, z^k) related to the k$^{\text{ème}}$ layer, their expressions are:

$$Q_{11} = \frac{E_1}{1 - v_{12}v_{21}}; \quad Q_{12} = \frac{v_{12}E_2}{1 - v_{12}v_{21}}; \quad Q_{22} = \frac{E_2}{1 - v_{12}v_{21}};$$
$$Q_{66} = G_{12}; \quad Q_{44} = G_{23} = G_{13}; \quad Q_{55} = G_{13} \quad (4)$$

In the case of plane stresses, the reduced rigidities require independent engineering constants as shown in Table 1 in the Appendix.

The in-plane forces per unit length acting on the plate edges in the x and y directions respectively are $F_x(y)$ and $F_y(x)$. Assume that the in-plane shear force per unit length xy is zero $F_{xy} = 0$. In this study, we'll take loads ($F_x(y)$ and $F_y(x)$) as:

$$F_x(y) = -F_0(1 - \alpha y/b) \quad \text{and} \quad F_y(x) = -F_0(1 - \beta x/a) \quad (5)$$

With, the intensity of the critical buckling load in the plane is F_0. The coefficients α and β are numbers chosen as $(\alpha, \beta = \{0, 1, 2\})$ and are called load parameters. Examples of possible uni-axial and bi-axial loading are given in Figures 2 and 3.

The coefficients of inertia of the plate are:

$$\{I_0, I_2\} = \int_{-\frac{h}{2}}^{\frac{h}{2}} \rho\{1, z^2\}dz \quad (6)$$

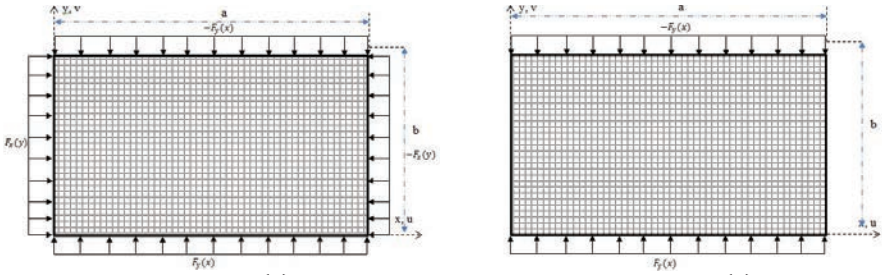

Example 1 : $F_x(y) = F_0$, $F_y(x) = F_0$ *Example* 2 : $F_x(y) = 0$, $F_y(x) = F_0$

Figure 2 Examples of uniform compression loading in the plane.

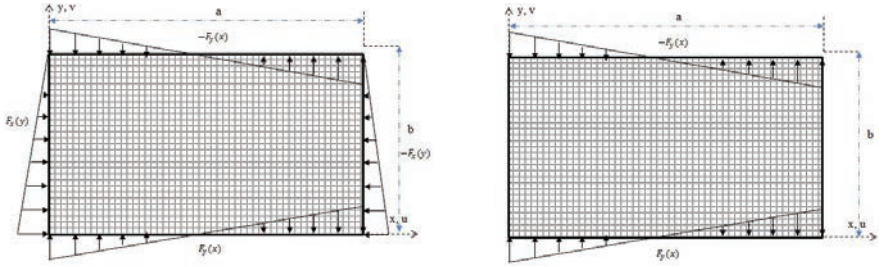

Figure 3 Examples of non-uniform loading in the plane.

2.2 Energy Formulation of the Buckling Problem

In the general case, we cannot formulate closed-form solutions of the Navier or Levy type for symmetrical rectangular plates in laminated composite materials that do not satisfy boundary conditions simply supported on at least two edges. Therefore, in this work, we seek semi-numerical solutions using the Ritz approximation. The deformation energy of a symmetrical laminated plate is given by.

$$U_d = \frac{1}{2}\iint [D_{11}(w_{,xx})^2 + 2D_{12}w_{,xx}w_{,yy} + D_{22}(w_{,yy})^2 + 4(D_{16}w_{,xx} + D_{26}w_{,yy})w_{,xy} + D_{66}(w_{,xy})^2]dxdy \tag{7}$$

The virtual work of the forces applied to the edges in the plane is:

$$V_P = \frac{1}{2}\iint [F_x(w_{,x})^2 + F_y(w_{,y})^2]dxdy \tag{8}$$

The kinetic energy of the plate is:

$$E_c = \frac{1}{2}\iint [I_1\ddot{w} - I_3(\ddot{w}_{,xx} + \ddot{w}_{,yy})]\delta w dxdy \tag{9}$$

The statement of the principle of minimum total potential energy of the buckling problem in the dynamic case is:

$$\delta\Pi(w(x,y)) = \delta\int_{t_i}^{t_f}(U_d - V_P - E_c)dt = 0 \tag{10}$$

Substituting Equations (7), (8) and (9) into (10) gives:

$$\begin{aligned}\delta\Pi(w(x,y)) = \int_0^b \int_0^a \{&D_{11}w_{,xx}\delta w_{,xx} + D_{12}(w_{,yy}\delta w_{,xx} + w_{,xx}\delta w_{,yy}) \\ &+ D_{22}w_{,yy}\delta w_{,yy} + 4D_{66}w_{,xy}\delta w_{,xy} \\ &+ 2D_{16}(w_{,xy}\delta w_{,xx} + w_{,xx}\delta w_{,xy}) \\ &+ 2D_{26}(w_{,xy}\delta w_{,yy} + w_{,yy}\delta w_{,xy}) + F_x w_{,x}\delta w_{,x} \\ &+ F_{xy}(w_{,y}\delta w_{,x} + w_{,x}\delta w_{,y}) + F_y w_{,y}\delta w_{,y}\} dxdy \\ &- I_0(w\delta w)_{,t} - I_2(w_{,x}\delta w_{,x} + w_{,y}\delta w_{,y})_{,t} \end{aligned} \tag{11}$$

2.3 Treated Boundary Conditions

In the present study we use so-called beam functions $X_r(x)$ and $Y_s(y)$ which satisfy at least the geometric boundary conditions:

Case 1: Simply supported at $x = 0, a$ and simply supported at $y = 0, b$

$$\begin{aligned} X_r(x) &= \sin(r\pi y/a) \\ Y_s(y) &= \sin(s\pi y/b) \end{aligned} \tag{12}$$

Case 2: Flush-mounted $x = 0, a$ and simply supported at $y = 0, b$

$$\begin{aligned} X_r(x) &= \sin(\lambda_r x/a) - sinh(\lambda_r x/a) + \alpha_r(\cosh(\lambda_r x/a) - cos(\lambda_r x/a)) \\ Y_s(y) &= \sin(s\pi y/b) \end{aligned} \tag{13}$$

Case 3: Free to $x = 0, a$ and simply supported by $y = 0, b$

$$\begin{aligned} X_r(x) &= \sin(\lambda_r x/a) + sinh(\lambda_r x/a) - \alpha_r(\cosh(\lambda_r x/a) + cos(\lambda_r x/a)) \\ Y_s(y) &= \sin(s\pi y/b) \end{aligned} \tag{14}$$

These basis functions verify the boundary conditions in $x = 0$ and $y = 0$. But we still have to satisfy the boundary conditions in $x = a$ and $y = b$ to be verified:

$$\cos(\lambda_r)\cosh(\lambda_r) = 1 \tag{15}$$

$$\alpha_r = (\sinh(\lambda_r) - sin(\lambda_r))/(\cosh(\lambda_r) - sos(\lambda_r)) \tag{16}$$

The parameters λ_r and α_r are illustrated in Table 2 in Appendix.

3 Numerical Formulation of the Problem

We will approximate the harmonic solution sought by the following series according to the Ritz approximation:

$$w(x,y) = \sum_{m=1}^{M}\sum_{n=1}^{N} W_{mn} e^{-j\omega t} X_m(x) Y_n(y) \tag{17}$$

Knowing ω is the free vibration pulsation of the plate and that the functions $X_m(x)$ and $Y_n(y)$ constructs a functional basis and are selected after its verification of the essential (or geometric) boundary conditions. The terms W_{mn} terms are then determined after the stationarity conditions have been applied:

$$\frac{\partial \widetilde{\Pi}}{\partial W_{mn}} = 0 \tag{18}$$

After explaining all the terms making up the expression of the deformation energy and the work of the forces applied to the edges, as well as the kinetic energy, we obtain:

$$\begin{aligned}
&\sum_{i=1}^{M}\sum_{j=1}^{N}\Bigg\{\int_{x=0}^{a}\int_{y=0}^{b}[D_{11}X_{m,xx}X_{i,xx}Y_nY_j + 4D_{66}X_{m,x}X_{i,x}Y_{n,y}Y_{j,y} \\
&\quad + D_{12}(X_{m,xx}X_iY_nY_{j,yy} + X_mX_{i,xx}Y_{n,yy}Y_j) + D_{22}X_mX_iY_{n,yy}Y_{j,yy} \\
&\quad + 2D_{16}(X_{m,xx}X_{i,x}Y_nY_{j,y} + X_{m,x}X_{i,xx}Y_{n,y}Y_j) \\
&\quad + 2D_{26}(X_mX_{i,x}Y_{n,yy}Y_{j,y} + X_{m,x}X_iY_{n,y}Y_{j,yy})]dxdy\Bigg\}W_{ij} \\
&\quad - \sum_{i=1}^{M}\sum_{j=1}^{N}\Bigg\{\int_{x=0}^{a}\int_{y=0}^{b}[F_xX_{m,x}X_{i,x}Y_nY_j \\
&\quad + F_yX_mX_iY_{n,y}Y_{j,y}]dxdy\Bigg\}W_{ij} \\
&\quad - \omega^2\sum_{i=1}^{M}\sum_{j=1}^{N}\Bigg\{\int_{x=0}^{a}\int_{y=0}^{b}[I_0X_mX_iY_nY_j \\
&\quad + I_2(X_{m,x}X_{i,x}Y_nY_j + X_mX_iY_{n,y}Y_{j,y})]dxdy\Bigg\}W_{ij} = 0
\end{aligned} \tag{19}$$

For $m \in \{1, 2, 3, \ldots, M\}$ and $n \in \{1, 2, 3, \ldots, N\}$.

To make it easier to write programs in MATLAB, we can simplify Equation (19) into a more compact form, such as the following:

$$\begin{aligned}
&\sum_{i=1}^{M}\sum_{j=1}^{N}[D_{11}k_{minj}^{2200} + 4D_{66}k_{minj}^{1111} + D_{12}(k_{minj}^{2002} + k_{minj}^{0220}) + D_{22}k_{minj}^{0022} \\
&\quad + 2D_{16}(k_{minj}^{2101} + k_{minj}^{1210}) + 2D_{26}(k_{minj}^{0121} + k_{minj}^{1012})]W_{ij} \\
&\quad - F_0\sum_{i=1}^{M}\sum_{j=1}^{N}[g(\alpha)_{minj}^{1100} + g(\beta)_{minj}^{0011}]W_{ij} \\
&\quad - \omega^2\sum_{i=1}^{M}\sum_{j=1}^{N}[I_0 m_{minj}^{0000} + I_2(m_{minj}^{1100} + m_{minj}^{0011})]W_{ij} \qquad (20)
\end{aligned}$$

For $m \in \{1, 2, 3, \ldots, M\}$ and $n \in \{1, 2, 3, \ldots, N\}$.

Knowing that the terms k_{minj}^{rspq}, $g(\alpha)_{minj}^{rspq}$, $g(\beta)_{minj}^{rspq}$ and m_{minj}^{rspq} are respectively expressed as:

$$k_{minj}^{rspq} = \int_{x=0}^{a}\frac{\partial^r X_m}{\partial x^r}\frac{\partial^s X_i}{\partial x^s}dx\int_{y=0}^{b}\frac{\partial^p Y_n}{\partial y^p}\frac{\partial^q Y_j}{\partial y^q}dy \qquad (21)$$

$$\begin{aligned}
g(\alpha)_{minj}^{rspq} &= \int_{x=0}^{a}\frac{\partial^r X_m}{\partial x^r}\frac{\partial^s X_i}{\partial x^s}dx \\
&\quad \times \int_{y=0}^{b}((-1+\alpha y/b))\frac{\partial^p Y_n}{\partial y^p}\frac{\partial^q Y_j}{\partial y^q}dy^2 \qquad (22)
\end{aligned}$$

$$\begin{aligned}
g(\beta)_{minj}^{rspq} &= \int_{x=0}^{a}((-1+\beta x/a))\frac{\partial^r X_m}{\partial x^r}\frac{\partial^s X_i}{\partial x^s}dx \\
&\quad \times \int_{y=0}^{b}\frac{\partial^p Y_n}{\partial y^p}\frac{\partial^q Y_j}{\partial y^q}dy \qquad (23)
\end{aligned}$$

$$m_{minj}^{rspq} = \int_{x=0}^{a}\frac{\partial^r X_m}{\partial x^r}\frac{\partial^s X_i}{\partial x^s}dx\int_{y=0}^{b}\frac{\partial^p Y_n}{\partial y^p}\frac{\partial^q Y_j}{\partial y^q}dy \qquad (24)$$

[2]The coefficients α and β determine the nature of the loading in the plane, uniform or non-uniform

The system of Equations (20) is made up of MN linear algebraic equations. MN possible modes. The discrete form (20) of the system governing motion can be written in matrix form, as:

In the case of buckling stability analysis (all displacements are independent of time):

$$[K]\{W\} - F_0[G]\{W\} = \{0\} \tag{25}$$

In the case of free vibration (no loading):

$$[K]\{W\} - \omega^2[M]\{W\} = \{0\} \tag{26}$$

The preceding systems (25) and (26) lead to the following eigenvalue problems:

$$([K] - F_0[G])\{W\} = \{0\} \tag{27}$$

$$([K] - \omega^2[M])\{W\} = \{0\} \tag{28}$$

In these forms of the eigenvalue problem, the symmetrical square plate stiffness matrix $[K]_{MN}$ is:

$$[K] = \begin{bmatrix} K_{1111} & \cdots & K_{111N} & \cdots & K_{1i1j} & \cdots & K_{1M11} & \cdots & K_{1M1N} \\ \vdots & \ddots & \ddots & \ddots & \ddots & \ddots & \ddots & \ddots & \vdots \\ K_{11N1} & \cdots & K_{11NN} & \cdots & K_{1iNj} & \ddots & K_{1MN1} & \cdots & K_{1MNN} \\ \vdots & \ddots & \ddots & \ddots & \ddots & \ddots & \ddots & \cdots & \vdots \\ K_{m1n1} & \cdots & K_{m1nN} & \cdots & \boldsymbol{K_{minj}} & \cdots & K_{mMn1} & \cdots & K_{mMnN} \\ \vdots & \ddots & \ddots & \ddots & \ddots & \ddots & \ddots & \ddots & \vdots \\ K_{M111} & \cdots & K_{M11N} & \cdots & K_{Mi1j} & \cdots & K_{MM11} & \cdots & K_{MM1N} \\ \vdots & \ddots & \ddots & \ddots & \ddots & \ddots & \ddots & \ddots & \vdots \\ K_{M1N1} & \cdots & K_{M1NN} & \cdots & K_{MiNj} & \cdots & K_{MMN1} & \cdots & K_{MMNN} \end{bmatrix} \tag{29}$$

Calculation of the terms K_{minj} is based on the integrals (21), with:

$$\begin{aligned} K_{minj} = {} & D_{11}k^{2200}_{minj} + 4D_{66}k^{1111}_{minj} + D_{12}(k^{2002}_{minj} + k^{0220}_{minj}) + D_{22}k^{0022}_{minj} \\ & + 2D_{16}(k^{2101}_{minj} + k^{1210}_{minj}) + 2D_{26}(k^{0121}_{minj} + k^{1012}_{minj}) \end{aligned} \tag{30}$$

The geometric square symmetric matrix of the plate $[G]_{MN}$ is:

$$[G] = \begin{bmatrix} G_{1111} & \cdots & G_{111N} & \cdots & G_{1i1j} & \cdots & G_{1M11} & \cdots & G_{1M1N} \\ \vdots & \ddots & \ddots & \ddots & \ddots & \ddots & \ddots & \ddots & \vdots \\ G_{11N1} & \cdots & G_{11NN} & \cdots & G_{1iNj} & \ddots & G_{1MN1} & \cdots & G_{1MNN} \\ \vdots & \ddots & \ddots & \ddots & \ddots & \ddots & \ddots & \cdots & \vdots \\ G_{m1n1} & \cdots & G_{m1nN} & \cdots & \boldsymbol{G_{minj}} & \cdots & G_{mMn1} & \cdots & G_{mMnN} \\ \vdots & \ddots & \ddots & \ddots & \ddots & \ddots & \ddots & \ddots & \vdots \\ G_{M111} & \cdots & G_{M11N} & \cdots & G_{Mi1j} & \cdots & G_{MM11} & \cdots & G_{MM1N} \\ \vdots & \ddots & \ddots & \ddots & \ddots & \ddots & \ddots & \ddots & \vdots \\ G_{M1N1} & \cdots & G_{M1NN} & \cdots & G_{MiNj} & \cdots & G_{MMN1} & \cdots & G_{MMNN} \end{bmatrix} \tag{31}$$

To obtain the coefficients G_{minj} the integrals (22) and (23) are used, with:

$$G_{minj} = g(\alpha)_{minj}^{1100} + g(\beta)_{minj}^{0011} \tag{32}$$

The square symmetrical mass matrix of the plate $[M]_{MN}$ is:

$$[M] = \begin{bmatrix} M_{1111} & \cdots & M_{111N} & \cdots & M_{1i1j} & \cdots & M_{1M11} & \cdots & M_{1M1N} \\ \vdots & \ddots & \ddots & \ddots & \ddots & \ddots & \ddots & \ddots & \vdots \\ M_{11N1} & \cdots & M_{11NN} & \cdots & M_{1iNj} & \ddots & M_{1MN1} & \cdots & M_{1MNN} \\ \vdots & \ddots & \ddots & \ddots & \ddots & \ddots & \ddots & \cdots & \vdots \\ M_{m1n1} & \cdots & M_{m1nN} & \cdots & \boldsymbol{M_{minj}} & \cdots & M_{mMn1} & \cdots & M_{mMnN} \\ \vdots & \ddots & \ddots & \ddots & \ddots & \ddots & \ddots & \ddots & \vdots \\ M_{M111} & \cdots & M_{M11N} & \cdots & M_{Mi1j} & \cdots & M_{MM11} & \cdots & M_{MM1N} \\ \vdots & \ddots & \ddots & \ddots & \ddots & \ddots & \ddots & \ddots & \vdots \\ M_{M1N1} & \cdots & M_{M1NN} & \cdots & M_{MiNj} & \cdots & M_{MMN1} & \cdots & M_{MMNN} \end{bmatrix} \tag{33}$$

Determining the terms M_{minj} is determined by calculating the integrals (24), with:

$$M_{minj} = I_0 m_{minj}^{0000} + I_2(m_{minj}^{1100} + m_{minj}^{0011}) \tag{34}$$

The column vector $\{W\}_{MNx1}$ of unknown deviations has the following transposed form:

$$\{W\} = \begin{Bmatrix} W_{11} & \cdots & W_{1N} & \cdots & W_{mn} & \cdots & W_{M1} & \cdots & W_{MN} \end{Bmatrix}^T \tag{35}$$

4 Numerical Results and Interpretation

The first is to quantify the effect of bending/torsion coupling in terms of the critical buckling load, and the second is to determine the contribution of this effect to the free vibration behavior of this type of plate. In the remainder of this study, we will accept approximately a 14-layer plate as a specially orthotropic[3] plate for any comparison made.

4.1 Formulation Validation

In order to determine the accuracy of the method adopted in this study and the convergence of the numerical formulation used, we record the critical buckling load and the fundamental free vibration frequency of a symmetrical laminated plate. To do this, a MATLAB program is run with a ratio of anisotropy E_1/E_2 and slenderness a/h for two schemes ($N_c = 4$ layers and $N_c = 12$ layers), and the results are listed in Table 3 in the Appendix.

To validate the theoretical method used, a comparison is made with the results obtained by ASHTON and WADDOUPS, who use experimental approaches in their studies [39]. According to Table 3, a good agreement can be observed between our results and those of Ashton and Waddoups for a 12-layer plate. However, to obtain acceptable accuracies for plates with a reduced number of layers, a large number of deformation modes of the plate must be taken into account. (m, n) of plate deformation, which immediately increases the stiffness matrices $[K]$ geometry $[G]$ and mass matrices $[M]$.

4.2 Effect of Bending/Torsion Coupling on Critical Buckling Load

We determine the effect of the number of layers $N_c = (4, 8, 12$ or 14 layers) on the critical buckling load of a symmetrical laminated plate simply supported on two parallel edges and free on the other two. In addition, two types of uniform and non-uniform loading are adopted. The results are shown in Table 4 in the Appendix.

Firstly, we need to agree on the method for quantifying the effect of coupling on stability. The principle is to increase the number of plate layers, i.e. by decreasing the flexural/torsional coupling stiffnesses, thereby bringing it closer to a specially orthotropic configuration (where the coupling stiffnesses are zero). So, according to the results in Table 4, a significant difference

[3]Where, the effect of bending/torsion coupling is absent $\mathrm{D}_{16} = \mathrm{D}_{26} = 0$.

between the critical buckling loads of the two plate configurations $N_c = 4$ and $N_c = 14$ (an error of more than 14% is made if we want to approximate the case $N_c = 4$ by the especially orthotropic plate configuration). This difference shows that bending/torsion coupling has a significant effect on buckling behavior for plates with a reduced number of layers. The error can reach 46.68% in the case of an anisotropy of $E_1/E_2 = 40$ and a slenderness ratio of $a/h = 25$. On the other hand, for a square boron-epoxy symmetrical plate with angular folds $\theta = 45°$ 12-layer uniaxially plane-loaded square boron-epoxy plate, the error on the critical buckling load is 0.49% when the specially orthotropic approximation is used, whereas this error becomes 1.45% for the same plate but with an anisotropy of $E_1/E_2 = 40$ and a slenderness ratio of $a/h = 25$. We note that the bending/torsion coupling effect disappears very rapidly as the number of layers increases.

Figure 4 shows the non-dimensional critical buckling load F_{cr} as a function of slenderness ratio a/h and Figure 5 shows the same load as a function of anisotropy E_1/E_2. The plate studied is a symmetrical laminate with angular folds whose angle of lamination is $\theta = 45°$ for different patterns $N_c = (4, 8, 12 \text{ or } 14 \text{ layers})$.

Figure 4 shows that the non-dimensional critical buckling load F_{cr} increases exponentially with increasing plate slenderness for $a/h \in [5, 30]$ the increase in this load is explained by the absence of the shear effect for higher ratios of a/h. This load approaches a fixed load when the anisotropy ratio E_1/E_2 continues to increase, as shown in Figure 5. We also note that for a plate of $N_c = 4$ layers plate, the buckling load is small but

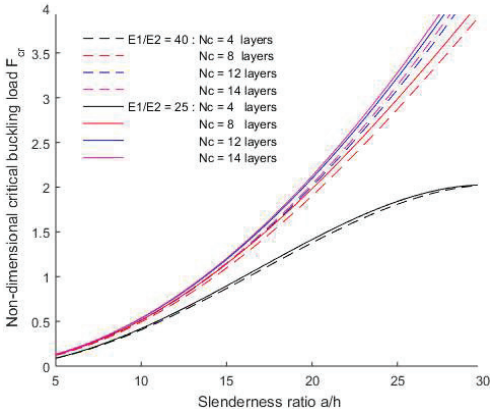

Figure 4 Non-dimensional critical buckling load as a function of the ratio a/h.

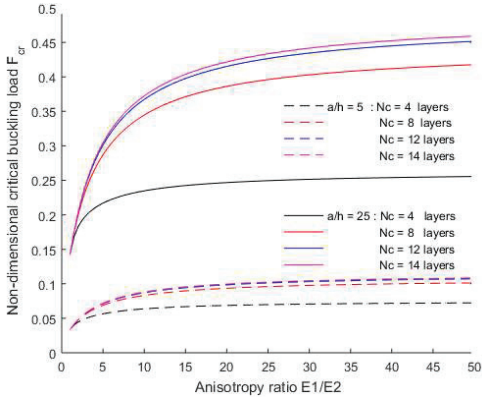

Figure 5 Non-dimensional critical buckling load as a function of anisotropy E_1/E_2.

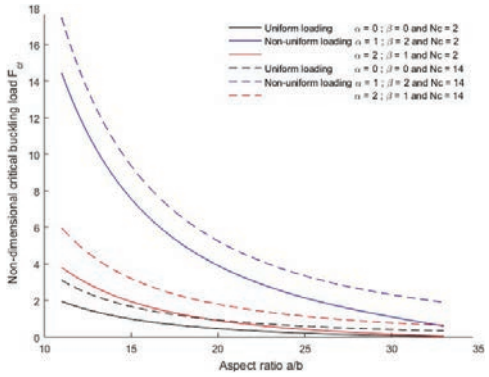

Figure 6 Simulation of non-dimensional critical buckling load F_{cr} as a function of a/b for both types of loading.[4]

increases with N_c and approaches the curve for the $N_c \geq 14$ layers case (which represents, approximately, the specially orthotropic configuration), this behavior justifying the absence of coupling between bending/torsion when N_c increases.

In Figure 6 we have drawn the curves representing the critical buckling load F_{cr} as a function of aspect ratio for uniform/non-uniform loading. Figure 7 shows the behavior of the symmetrical laminated plate in terms of elastic stability under three boundary conditions: simply supported, embedded or free.

[4] α and β Are load coefficients that determine the nature of the loading $F_x(y)$ and $F_y(x)$ uniform or non-uniform, as specified in the previous sections.

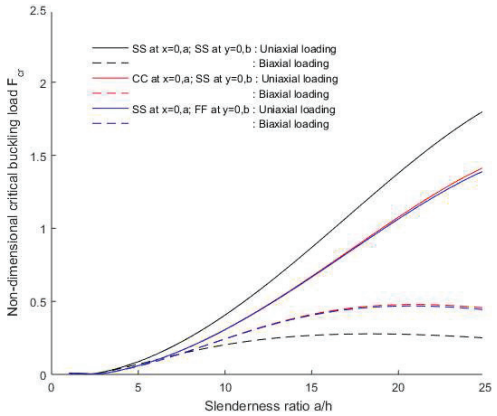

Figure 7 Simulation of the non-dimensional critical buckling load F_{cr} as a function of a/h for the three types of boundary conditions.[5]

The decrease in critical buckling load (illustrated in Figure 6) is clear with increasing aspect ratio, but it is also concluded that the plate bends faster under uniform loads with two layers and resists better against non-uniform loads. ($\alpha = 1$ and $\beta = 2$). Figure 7 shows that when the plate has a small aspect ratio ($a/h < 5$) the boundary conditions have almost the same effect on the buckling load of a laminated plate with angular folds, but if this ratio is larger we need to be careful when analyzing problems with varying boundary conditions.

The variation of the critical buckling load as a function of the lamination angle θ is shown in Figures 8 and 9. Figure 8 illustrates the effect of loading type (un-axial or bi-axial) for the different lamination patterns, while Figure 9 shows the buckling behavior for the three types of boundary conditions.

Irrespective of slenderness and aspect ratio, the critical buckling load of a symmetrical laminated plate increases as the angle of lamination is varied from 0° to 45° and decreases for a continuous and increasing variation of the angle from θ From 45° to 90°, this applies to a symmetrical angle-ply laminated plate with simply supported boundary conditions and biaxial loading in the planes. The approximation of critical buckling load values to that of a specially orthotropic plate (the 14-layer case), is clear from the results drawn in Figure 8. Furthermore, the lowest and highest loads correspond to the cases of plates ($SSSS$ and $N_c = 2$ layers) and $CCSS$ and $N_c = 14$ layers respectively, as shown in Figure 9. This behavior can be

[5]SS: simply supported, CC: clamped and FF: free.

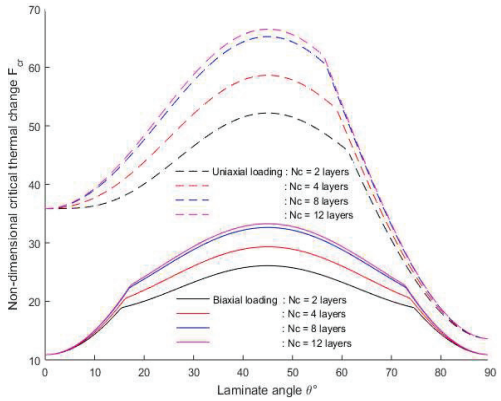

Figure 8 F_{cr} as a function of lamination angle θ for different types of loading.

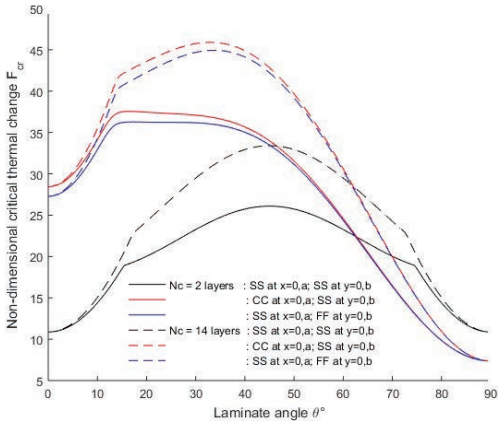

Figure 9 F_{cr} as a function of lamination angle θ for different types of boundary conditions.

explained by the fact that higher stresses on the plate boundaries increase the plate's transverse stiffness, which makes the plate's buckling response higher.

4.3 Effect of Bending/Torsion Coupling on Free Vibration

The natural frequencies of the fundamental mode ($m = 1, n = 1$) for the free vibration analysis of symmetrical laminated plates are presented in Table 5. The analysis is carried out for the three types of boundary conditions (SS, CC and/or FF), and we have processed 4 schemes ($N_c = 4, 8, 12$ or 14 layers) in order to quantify the effect of bending/torsion coupling on the free vibration of the structure.

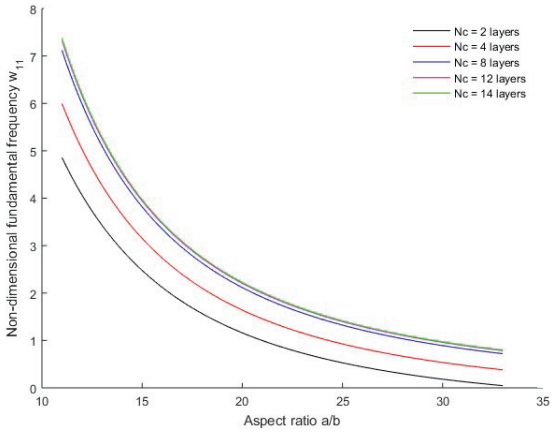

Figure 10 Fundamental frequency as a function of aspect ratio for different lamination patterns.

According to Table 5, approximating the case where ($N_c = 2$ layers) by a specially orthotropic plate leads to a relative error of 64.08% in the case of an anisotropy ratio of $E_1/E_2 = 40$ and an aspect ratio of $a/b = 10$. This error drops to 1.21% for $N_c = 12$ layers. We note that the bending/torsion coupling effect disappears very quickly as the number of layers increases.

Figure 10 shows the fundamental free vibration frequency of an angularly ply laminated plate with simply supported edges as a function of aspect ratio a/b. A comparison between the fundamental frequencies for the three types of boundary conditions treated in this study (simply supported, fixed or free) as a function of plate anisotropy is presented in Figure 11.

The fundamental frequency of free vibration of a symmetrical laminated plate decreases as the aspect ratio increases and also as the number of layers becomes small, this remark is valid for an angularly folded symmetrical laminated plate with simply supported boundary conditions and uniaxial loading in the planes, the convergence of the critical buckling load towards that of a specially orthotropic plate is very clear from the results presented in Figure 10. Furthermore, the lowest and highest frequencies correspond, respectively, to the cases of plates ($SSSS$ and $N_c = 14$ layers) and $CCSS$ and $N_c = 4$ layers respectively, as shown in Figure 11.

Figure 12 shows the fundamental free vibration frequency as a function of lamination angle θ for two lamination schemes ($N_c = 4$ and 14 layers). In order to see the effect of bending/torsion coupling of a laminated plate with angular folds on the free vibration, this study is carried out with three aspect

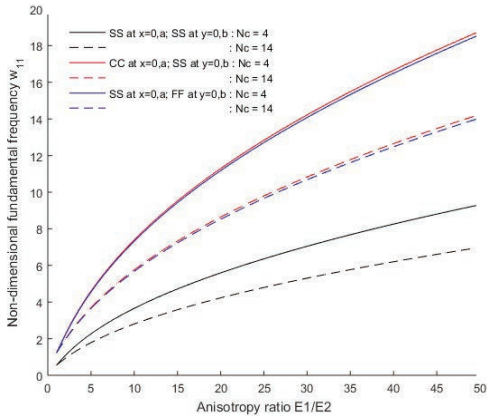

Figure 11 Fundamental frequency as a function of the anisotropy ratio for different types of boundary conditions.

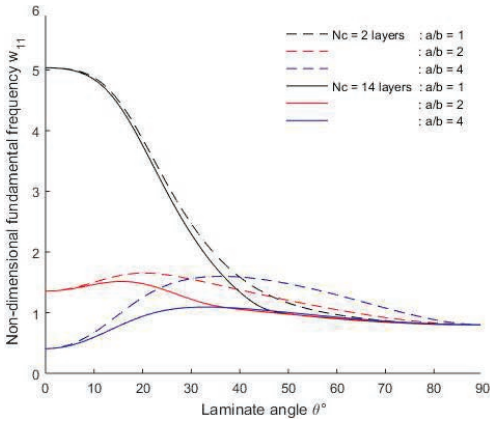

Figure 12 Fundamental frequency as a function of lamination angle for different aspect ratios.

ratios. Figure 13 shows the same behavior of the same plate, but in this case we change the anisotropy. E_1/E_2.

According to Figures 12 and 13, the fundamental free-vibration frequencies of an angularly-folded symmetrical laminated plate decrease for lamination angles greater than 25°, irrespective of the plate's anisotropy and aspect ratios. The effect of bending/torsion coupling is most significant for lamination angles around 45°, and becomes absent for angle 0° (especially orthotropic plates) and 90° (symmetrical cross-ply plates).

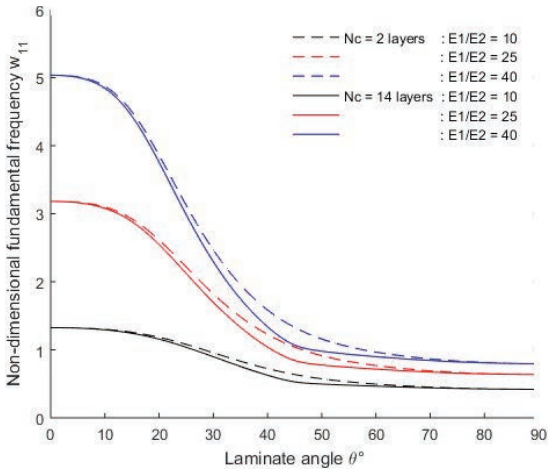

Figure 13 Fundamental frequency as a function of lamination angle for different anisotropy ratios.

5 Conclusion

In this study, bending/torsion coupling was analyzed with different parameters in a symmetrical laminated composite plate with angular folds, reducing the effective bending and bending/torsion stiffnesses. As a result, the critical buckling load decreases and the fundamental free vibration frequency increases. The effect of this coupling on the buckling load for a symmetrical laminate rapidly disappears as the number of layers increases, but for less than fourteen layers we cannot neglect this effect. As the lamination angle approaches 45°, the critical buckling load takes on its maximum value, whereas it decreases for symmetrical laminates with angular folds as the aspect ratio increases. The increase in plate anisotropy makes the critical buckling load and the fundamental frequency of free vibration greater. As a general rule, engineers should be very cautious about approximating the behavior of an angle-ply symmetrical laminated composite plate to that of a specially orthotropic plate in the case of plates with fewer than 14 layers.

Acknowledgements

The support given to this research project by Sidi Mohamed Ben Abdellah University of Fez is gratefully acknowledged. The author would also like to thank the professors at ENS Fès for their help in correcting the manuscript.

Appendix

Table 1 Engineering constant values for materials* [2]

Material Properties	E_1	E_2	G_{12}	G_{13}	v_{12}
Graphite – Epoxy	*20.0*	*1.3*	*1.03*	*0.90*	*0.30*
Boron – Epoxy	*30.0*	*3.0*	*1.00*	*0.60*	*0.30*

*Moduli are expressed in msi = million psi;
1 psi = 6,894.76 N/m^2 ; Pa = N/m^2 ; kPa = 10^3 Pa;
MPa = 10^6 Pa; GPa = 10^9 Pa.

Table 2 Values λ_r and α_r verifying boundary conditions

r	1	2	3	4	5	6	7	8
λ_r	4,73004	7,85320	10,99560	14,13716	17,27875	20,42035	23,56194	26,70353
α_r	0,982502	1,000777	0,999966	1,000001	0,999999	1,000000	1,000000	1,000000

Table 3 Validation of theoretical results

			$N_c = 4$ layers			$N_c = 14$ layers*		
Size Measured	E_1/E_2	a/h	Present	Ref [39]	Error	Present	Ref [39]	Error
Critical	5	10	0.3083	0,3002	2,70%	0.3589	0,3534	1,56%
buckling		25	1.5729	1,5859	0,82%	2.2050	2,2025	0,11%
load	40	10	0.4200	0,4285	1,98%	0.5377	0,5302	1,41%
F_{cr}		25	1.8413	1,8154	1,43%	3.2792	3,2424	1,13%
Fundamental	5	10	2.2270	2,2240	0,13%	1.8187	1,8187	0,00%
free		25	2.5175	2,5895	2,78%	1.9156	1,9175	0,10%
vibration	40	10	8.0637	7,9921	0,90%	6.3161	6,3685	0,82%
frequency ω_{11}		25	9.2989	9,1245	1,91%	6.7225	6,6425	1,20%

*The case where $N_c = 14$ layers will be treated in the following, approximately, as a specially orthotropic plate.

Table 4 The critical buckling load F_{cr} of a symmetrical laminated plate as a function of anisotropy, aspect ratio and slenderness

Load Type		Uni-Axial Loading				Bi-Axial Loading			
E_1/E_2		5		40		5		40	
a/h		10	25	10	25	10	25	10	25
$N_c = 4$ layers		0.2443	1.2924	0.3162	1.4383	0.1952	0.4260	0.2512	0.4588
	Error[1]	14.55%	26.56%	23.65%	43.31%	14.87%	26.96%	24.96%	46.68%
$N_c = 8$ layers		0.2781	1.6736	0.3957	2.3317	0.2231	0.5606	0.3194	0.7991
	Error	2.72%	4.90%	4.45%	8.10%	2.73%	3.88%	4.58%	7.13%
$N_c = 12$ layers		0.2845	1.7443	0.4108	2.5003	0.2282	0.5793	0.3320	0.8502
	Error	0.49%	0.88%	0.80%	1.45%	0.49%	0.68%	0.82%	1.19%
$N_c = 14$ layers[2]		0.2859	1.7599	0.4142	2.5374	0.2294	0.5833	0.3348	0.8605

[1]Relative error is calculated by $Error\% = 100.(F_{cr}(N_c = 14 \text{ layers}) - F_{cr}(N_c))/F_{cr}(N_c = 14 \text{ layers})$ for a plate of N_c layers.
[2]The shaded line is reserved for the case representing a specially orthotropic plate.

Table 5 Effect of boundary conditions on the contribution of bending/torsion coupling to the fundamental frequency ${}^1\omega_{11}$ of a symmetrical laminated plate

Number of Layers N_c		a/b	SS at $x=0,a$ SS at $y=0,b$ $E_1/E_2=5$	SS at $x=0,a$ SS at $y=0,b$ $E_1/E_2=40$	CC at $x=0,a$ SS at $y=0,b$ $E_1/E_2=5$	CC at $x=0,a$ SS at $y=0,b$ $E_1/E_2=40$	CC at $x=0,a$ FF at $y=0,b$ $E_1/E_2=5$	CC at $x=0,a$ FF at $y=0,b$ $E_1/E_2=40$
2 layers		2	0.7585	4.8549	1.8029	11.7057	1.7764	11.5531
	Error		21.66%	34.19%	18.16%	29.52%	17.96%	29.22%
12 layers			0.9645	7.3309	2.1958	16.5181	2.1584	16.2357
	Error		0.39%	0.63%	0.33%	0.54%	0.32%	0.53%
14 layers			0.9683	7.3773	2.2031	16.6087	2.1655	16.3237
2 layers		10	0.1597	0.8566	0.3285	1.4462	0.3252	1.4467
	Error		33.85%	53.29%	39.97%	64.70%	39.55%	64.08%
12 layers			0.2400	1.8160	0.5431	4.0473	0.5340	3.9792
	Error		0.62%	0.99%	0.74%	1.23%	0.73%	1.21%
14 layers			0.2415	1.8343	0.5472	4.0977	0.5379	4.0282

Fundamental pulsation and frequency are linked by $\omega_{11} = 2\pi f_{11}$.

References

[1] Autar K. Kaw; Mechanics of composite materials second edition; (2006), International Standard Book Number-13: 978-0-8493-1343-1.

[2] J. N. Reddy (2003) ; Mechanics of Laminated Composite Plates and Shells, 2nd Edition; eBook ISBN: 9780429210693; https://doi.org/10.1201/b12409.

[3] Kadoli R. and Ganesan, N. (2006). Buckling and free vibration analysis of functionally graded cylindrical shells subjected to a temperature-specified boundary condition. Journal of Sound and Vibration, 289(3), 450–480. http://doi:10.1016/j.jsv.2005.02.034.

[4] Do, V. N. V. and Lee C. H. (2017). Thermal buckling analyses of FGM sandwich plates using the improved radial point interpolation mesh-free method. Composite Structures, 177, 171 186. http://doi:10.1016/j.compstruct.2017.06.054.

[5] Adhikari, B., Dash P. and Singh B. N. (2020). Buckling analysis of porous FGM sandwich plates under various types nonuniform edge compression based on higher order shear deformation theory. Composite Structures, 112597. http://doi:10.1016/j.compstruct.2020.112597.

[6] Singh, S. J. and Harsha S. P. (2020). Thermo-mechanical analysis of porous sandwich S-FGM plate for different boundary conditions using Galerkin Vlasov's method: A semi-analytical approach. Thin-Walled Structures, 150, 106668. http://doi:10.1016/j.tws.2020.106668.

[7] Adim, B., Daouadji T. H., Abbes B. and Rabahi, A. (2016). Buckling and free vibration analysis of laminated composite plates using an

efficient and simple higher order shear deformation theory. Mechanics & Industry, 17(5), 512. http://doi:10.1051/meca/2015112.

[8] Ounis, H., Tati, A., and Benchabane, A. (2014). Thermal buckling behavior of laminated composite plates: a finite-element study. Frontiers of Mechanical Engineering, 9(1), 41–49. http://doi:10.1007/s11465-014-0284-z.

[9] Civalek Ö., Dastjerdi, S. and Akgöz B. (2020). Buckling and free vibrations of CNT-reinforced cross-ply laminated composite plates. Mechanics Based Design of Structures and Machines, 1–18. http://doi:10.1080/15397734.2020.1766494.

[10] Nguyen-Van H., Mai-Duy N., Karunasena W. and Tran-Cong T. (2011). Buckling and vibration analysis of laminated composite plate/shell structures via a smoothed quadrilateral flat shell element with in-plane rotations. Computers & Structures, 89(7–8), 612–625. http://doi:10.1016/j.compstruc.2011.01.005.

[11] Akavci S. S. (2007). Buckling and Free Vibration Analysis of Symmetric and Antisymmetric Laminated Composite Plates on an Elastic Foundation. Journal of Reinforced Plastics and Composites, 26(18), 1907–1919. http://doi:10.1177/0731684407081766.

[12] Golmakani M. E., Esmaeilzadeh, M., Sadeghian, M. and Zeighami, V. (2021). Buckling analysis of CNTRC plates in the thermal environment based on combination of the incremental load technique and dynamic relaxation method. International Journal for Computational Methods in Engineering Science and Mechanics, 22(4), 316–332. http://doi:10.1080/15502287.2021.1882615.

[13] Civalek, Ö. and Avcar, M. (2020). Free vibration and buckling analyses of CNT reinforced laminated non-rectangular plates by discrete singular convolution method. Engineering with Computers. http://doi:10.1007/s00366-020-01168-8.

[14] Khandelwal R. P., Chakrabarti A. and Bhargava P. (2013). Vibration and buckling analysis of laminated sandwich plate having soft core. International Journal of Structural Stability and Dynamics, 13(08), 1350034. http://doi:10.1142/s021945541350034x.

[15] Kurpa, L. and Shmatko, T. (2020). Buckling and free vibration analysis of functionally graded sandwich plates and shallow shells by the Ritz method and the R-functions theory. Proceedings of the Institution of Mechanical Engineers, Part C: Journal of Mechanical Engineering Science, 095440622093630. http://doi:10.1177/0954406220936304.

[16] Yekani, S. M. A. and Fallah, F. (2020). A Levy solution for bending, buckling, and vibration of Mindlin micro plates with a modified couple stress theory. SN Applied Sciences, 2(12). http://doi:10.1007/s42452-020-03939-w.

[17] Peng, L. X., Liew, K. M., and Kitipornchai, S. (2006). Buckling and free vibration analyses of stiffened plates using the FSDT mesh-free method. Journal of Sound and Vibration, 289(3), 421–449. http://doi:10.1016/j.jsv.2005.02.023.

[18] Festus Chukwudi Onyeka, Chidobere David Nwa-David, Thompson Edozie Okeke, (2022); Study on Stability Analysis of Rectangular Plates Section Using a Three-Dimensional Plate Theory with Polynomial Function; Journal of Engineering Research and Sciences, 1(4): 28–37, 2022; https://dx.doi.org/10.55708/js0104004.

[19] Trabelsi S., Zghal, S. and Dammak F. (2020). Thermo-elastic buckling and post-buckling analysis of functionally graded thin plate and shell structures. Journal of the Brazilian Society of Mechanical Sciences and Engineering, 42(5). http://doi:10.1007/s40430-020-02314-5.

[20] Rasid, Z. A. and Yahaya H. (2014). The Thermal Instability Analysis of Functionally Graded Carbon Nanotube Composite Plates Using Finite Element Method. Applied Mechanics and Materials, 695, 285–288. http://doi:10.4028/www.scientific.net/amm.695.285.

[21] Bouazza M., Becheri T., Boucheta A. and Benseddiq N. (2016). Thermal buckling analysis of nanoplates based on nonlocal elasticity theory with four-unknown shear deformation theory resting on Winkler-Pasternak elastic foundation. International Journal for Computational Methods in Engineering Science and Mechanics, 17(5–6), 362–373. http://doi:10.1080/15502287.2016.1231239.

[22] Lal, A., Kulkarni N. M. and Singh B. N. (2015). Stochastic Thermal Post Buckling Response of Elastically Supported Laminated Piezoelectric Composite Plate Using Micromechanical approach. Curved and Layered Structures, 2(1). http://doi:10.1515/cls-2015-0019.

[23] Foroutan K., Shaterzadeh, A. and Ahmadi H. (2019). Nonlinear static and dynamic hygrothermal buckling analysis of imperfect functionally graded porous cylindrical shells. Applied Mathematical Modelling. http://doi:10.1016/j.apm.2019.07.062.

[24] Qi Y. N., Dai H. L. and Deng S.-T. (2020). Thermoelastic analysis of stiffened sandwich doubly curved plate with FGM core under low velocity impact. Composite Structures, 253, 112826. http://doi:10.1016/j.compstruct.2020.112826.

[25] Trabelsi S., Zghal S. and Dammak F. (2020). Thermo-elastic buckling and post-buckling analysis of functionally graded thin plate and shell structures. Journal of the Brazilian Society of Mechanical Sciences and Engineering, 42(5). http://doi:10.1007/s40430-020-02314-5.

[26] Do V. N. V. and Lee C.-H. (2017). Thermal buckling analyses of FGM sandwich plates using the improved radial point interpolation mesh-free method. Composite Structures, 177, 171–186. http://doi:10.1016/j.compstruct.2017.06.054.

[27] Li D., Deng Z., Chen G., Xiao H. and Zhu L. (2017). Thermomechanical bending analysis of sandwich plates with both functionally graded face sheets and functionally graded core. Composite Structures, 169, 29–41. http://doi:10.1016/j.compstruct.2017.01.026.

[28] Abdoun F. and Azrar L. (2020). Thermal buckling and vibration of laminated composite plates with temperature dependent properties by an asymptotic numerical method. International Journal for Computational Methods in Engineering Science and Mechanics, 1–15. http://doi:10.1080/15502287.2020.1729899.

[29] Singh S. J. and Harsha S. P. (2020). Thermo-mechanical analysis of porous sandwich S-FGM plate for different boundary conditions using Galerkin Vlasov's method: A semi-analytical approach. Thin-Walled Structures, 150, 106668. http://doi:10.1016/j.tws.2020.106668.

[30] Yamna Belkhodja, Mohamed El Amine Belkhodja, Hamida Fekirini, Djamel Ouinas (2023); New quasi-three-, and two-dimensional trigonometric-cubic monomial HSDT for thermal buckling and thermo-mechanical bending analyses of FGM symmetrical/non-symmetrical sandwich plates with hard/soft core; Composite Structures (304) 116402, https://doi.org/10.1016/j.compstruct.2022.116402.

[31] Supen Kumar Sah, Anup Ghosh (2022); Influence of porosity distribution on free vibration and buckling analysis of multi-directional functionally graded sandwich plates; Composite Structures (279) 114795, https://doi.org/10.1016/j.compstruct.2021.114795.

[32] Al-Furjan M. S. H., Farrokhian A., Keshtegar B., Kolahchi R. and Trung N.-T. (2020). Higher order nonlocal viscoelastic strain gradient theory for dynamic buckling analysis of carbon nanocones. Aerospace Science and Technology, 107, 106259. http://doi:10.1016/j.ast.2020.106259.

[33] Robert M. Jones (1999); Mechanics of composite materials second edition; International Standard Book Number-13: 978-1-56032-712-7.

[34] Thai H.-T., Park M. and Choi, D.-H. (2013). A simple refined theory for bending, buckling, and vibration of thick plates resting on elastic

foundation. International Journal of Mechanical Sciences, 73, 40–52. http://doi:10.1016/j.ijmecsci.2013.03.017.

[35] Shahgholian D., Safarpour M., Rahimi A. R. and Alibeigloo, A. (2020). Buckling analyses of functionally graded graphene-reinforced porous cylindrical shell using the Rayleigh-Ritz method. Acta Mechanica. http://doi:10.1007/s00707-020-02616-8.

[36] Malikan M. and Eremeyev V. A. (2020). Post-critical buckling of truncated conical carbon nanotubes considering surface effects embedding in a nonlinear Winkler substrate using the Rayleigh-Ritz method. Materials Research Express. http://doi:10.1088/2053-1591/ab691c.

[37] Chen X., Nie G. and Wu Z. (2020). Application of Rayleigh-Ritz formulation to thermomechanical buckling of variable angle tow composite plates with general in-plane boundary constraint. International Journal of Mechanical Sciences, 106094. http://doi:10.1016/j.ijmecsci.2020.106094.

[38] Chwal M. and Muc, A. (2019). Buckling and Free Vibrations of Nanoplates - Comparison of Nonlocal Strain and Stress Approaches. Applied Sciences, 9(7), 1409. http://doi:10.3390/app9071409.

[39] J. F. Mandell (1968); Experimental Investigation of the Buckling of Anisotropic Fiber Reinforced Plastic Plates; Air Force Materials Laboratory Technical Report AFML-TR-68-281.

Biographies

Hafid Mataich, doctorant: Laboratory of Mathematics, Modeling and Applied Physics, High Normal School, Sidi Mohamed Ben Abbellah University, 30040 Fez, Morocco.

Bouchta El Amrani, professeur: Laboratory of Mathematics, Modeling and Applied Physics, High Normal School, Sidi Mohamed Ben Abbellah University, 30040 Fez, Morocco.